IEEE Access
Multidisciplinary | Rapid Review | Open Access Journal

Received 23 August 2023, accepted 17 October 2023, date of publication 23 October 2023, date of current version 2 November 2023.

Digital Object Identifier 10.1109/ACCESS.2023.3326822

APPLIED RESEARCH

Current Recycled and Self-Phase Shift to Expand the Length of Radio-Frequency Coils, With Application to Brain and Spine Coil Array at 7T MRI

DANIEL HERNANDEZ[1], DONGHYUK KIM[1], TAEWOO NAM[2], YONGHWA JEONG[1], MINYEONG SEO[1], EUNWOO LEE[3], JUNGHWAN KIM[4], AND KYOUNG-NAM KIM[3]

[1]Neuroscience Research Institute, Gachon University, Incheon 21988, South Korea
[2]Department of Health Sciences and Technology, GAIHST, Gachon University, Incheon 21999, South Korea
[3]Department of Biomedical Engineering, Gachon University, Seongnam 13120, South Korea
[4]Department of Radiology and EECS, University of Missouri-Columbia, Columbia, MO 65211, USA

Corresponding author: Kyoung-Nam Kim (kyoungnam.kim@gachon.ac.kr)

This work was supported by the Basic Science Research Program through the National Research Foundation of Korea (NRF) funded by the Ministry of Education under Grant 2021R1C1C1010003.

ABSTRACT The use of the 7-Tesla (T) magnetic resonance imaging (MRI) promises improved imaging quality and higher resolution compared with lower-field MRI systems. The design of the loop coil considers the tradeoff between coil size and performance. A larger coil enables deeper field penetration, but it may result in poorer field uniformity and localization. On the other hand, a smaller coil offers improved localization capabilities, however, field penetration reduces, and multiple coil elements are required to cover the same space as large coils. Additionally, safety concerns regarding the high-energy absorption of electromagnetic waves in healthy tissues principally limit the use of the 7T MRI, which is measured with the specific absorption rate (SAR). A coil that can generate a uniform magnetic field while maintaining a low SAR is necessary to comply with the SAR limits. We propose a coil design that recirculates the current and provides a phase shift in the same structure to provide a magnetic field over a broad area, thus reducing the number of channels required to cover the same area. We present electromagnetic (EM) simulations of the proposed coil with a magnetic field and SAR computed for the brain and human spine model. We built the coil and acquired images with a phantom using a 7T MRI system. The proposed coil improves the SAR by 43% compared with the reference coil in the spinal area in the case of EM simulations, indicating the imaging quality improvement potential of our proposed coil.

INDEX TERMS MRI, antennas, spine imaging, EM simulations.

I. INTRODUCTION

Magnetic resonance imaging (MRI) has become an essential diagnostic tool in medicine, allowing non-invasive imaging of biological structures and processes [1], [2]. MRI has revolutionized spinal imaging, allowing detailed assessment of spinal cord lesions and anomalies [3], [4], [5]. Spinal diseases, such as tumors, herniated discs, and spinal stenosis can cause pain, disability, and even paralysis, making accurate diagnosis and treatment essential. MRI offers high resolution and contrast, enabling early and accurate detection of spinal cord pathologies [6]. Advances in MRI technology, including stronger magnetic fields and improved coil designs, can enhance the sensitivity and specificity of spinal imaging, leading to better clinical outcomes. Over the years, significant advancements have been made in the field of magnetic resonance imaging (MRI) to enhance image quality and resolution. This has led to the emergence of higher magnetic field systems, including 7 Tesla (7T) MRI [7], [8], [9]. The utilization of 7T MRI scanners offers several

The associate editor coordinating the review of this manuscript and approving it for publication was Marco Giannelli.

advantages, most notably the ability to acquire images with higher spatial resolution, enabling detailed visualization of anatomical structures and improved diagnostic capabilities. While 7T MRI offers the potential for high-quality spinal imaging, it also poses certain challenges due to the higher frequency of electromagnetic waves utilized [10], [11], [12]. The non-uniformity of the magnetic field, resulting from the shortening of the wavelength, poses a significant limitation in 7T MRI. Furthermore, 7T MRI can lead to higher energy absorption by tissues, which must be taken into consideration. Consequently, safety concerns regarding the use of high-energy electromagnetic waves have recently been addressed, and approvals for brain imaging have been granted. However, further studies are still required to address safety concerns and optimize the technology for spinal and body imaging. Thus, this study designs a coil for spinal imaging at 7T MRI that optimizes the magnetic field uniformity while minimizing the specific absorption rate (SAR) of electromagnetic waves [13], [14], [15].

Several studies have focused on the advancement of radiofrequency coils, including loop coils and microstrips [16], [17], [18], [19], for their application in MRI. When it comes to transmission, coils capable of generating a uniform field and maintaining a low specific absorption rate (SAR) are preferred. On the other hand, for reception, coils with a high signal-to-noise ratio (SNR) are desirable [20], [21]. Consequently, it is important for the coils to be effectively decoupled to minimize correlated noise. Furthermore, the utilization of combined transmit/receive coils has demonstrated its utility in various imaging scenarios.

The relationship between the size of a loop coil with the produced magnetic B1 field and the SNR [20], [21] has been previous investigated; indicating that the penetration rate and SNR are proportional to the diameter of the coil [20], [22], [23], [24]. Hence, when it comes to imaging larger anatomical regions like the spine and torso, the necessity arises for larger coils capable of generating a B1 field at greater distances within the patient. However, the use of large coils introduces the challenge of producing non-uniform B1 fields, particularly at higher frequencies such as 300 MHz, which is employed in 7T MRI systems. Conversely, small coils have higher sensitivities and better spatial resolution [19], [20]. Moreover, they can be combined with additional coils to form arrays that provide parallel imaging capabilities for both transmission and reception [25], [26], [27]. Theoretically, increasing the number of channels would provide a better MR image. However, in practice, a large number of coils is disadvantageous in terms of the complexity of the structure, cable management, and coupling between coils. Furthermore, the number of channels is limited by the radio-frequency RF transmitter and the number of reception channels in the spectrometer [28].

This study investigates the use of a coil that can recirculate the current to provide a magnetic B1 field in a large area when compared with a single-loop coil while providing a similar B1 field with an array of loop coils. We investigate the use of the proposed design for brain and spinal imaging. We performed electromagnetic simulations to determine the geometry and coil performance, build the coil, and test it by acquiring images using a 7T MRI scanner. We compare the proposed coil with a conventional loop-array coil arrangement.

II. METHODS

A. RF COIL DESIGN AND SIMULATIONS

The proposed coil is an extension of the circular loop coil that incorporates several adjacent circular paths. The central coil was divided into two semicircles, creating a gap in which an adjacent semicircle was added to allow the current to flow in the same direction. Capacitors were placed at both ends of the structure to return the current from the semicircles. The 3D model and geometry of the proposed coil are shown in Fig. 1a. The coil is constructed as a circular shape with a radius r and a specified number n of cycles tn. Capacitors are strategically positioned within the coil as depicted in the illustration. While the overall geometry of the coil resembles an array of circular loop coils arranged along the perimeter, the proposed coil does not require capacitors to connect and complete individual loops. The current flow within this structure is carefully designed to ensure that the phase of each individual turn contributes constructively to the overall magnetic field. The direction of the current flow is indicated by arrows in Figure 1a. We conducted three analyses based on an electromagnetic simulation to demonstrate the effectiveness of the proposed coil. The first analysis is a comparison between a single channel of the recycle self-phase-shift current coil (which will be referred as recycle-coil), a large rectangular coil, and an array of three channels with the same geometry as the recycle-coil. The term ''self-phase'' denotes the capacity of the coil's geometry to generate a current flow closely resembling the current distribution that an array of individual loop coils would produce, with controlled phase differences, in order to attain a uniform B1 field. The second analysis was an implementation brain array using the recycle-coil with the comparison of a standard loop array coil. The third analysis was based on a spine array coil, in which the recycle-coil was compared with a planar loop array.

Electromagnetic (EM) simulations were performed using commercial software (Sim4Life ZMT, https://www.zmt.swiss). The coils were excited with a Gaussian pulse input voltage source of 300 MHz central frequency and 600 MHz bandwidth; every conductor line was treated as a perfect electrical conductor. The EM simulations magnetic B1 field and SAR maps were computed. Each port was tuned and matched to 50 Ω using an LC network circuit.

A human model (DUKE) provided by the simulation software [29] was used to compute the B1 field and SAR maps for each coil configuration. This model comprised 72 tissues, bones, and organs with high detail. The model also provided electrical properties, such as conductivity and permittivity for

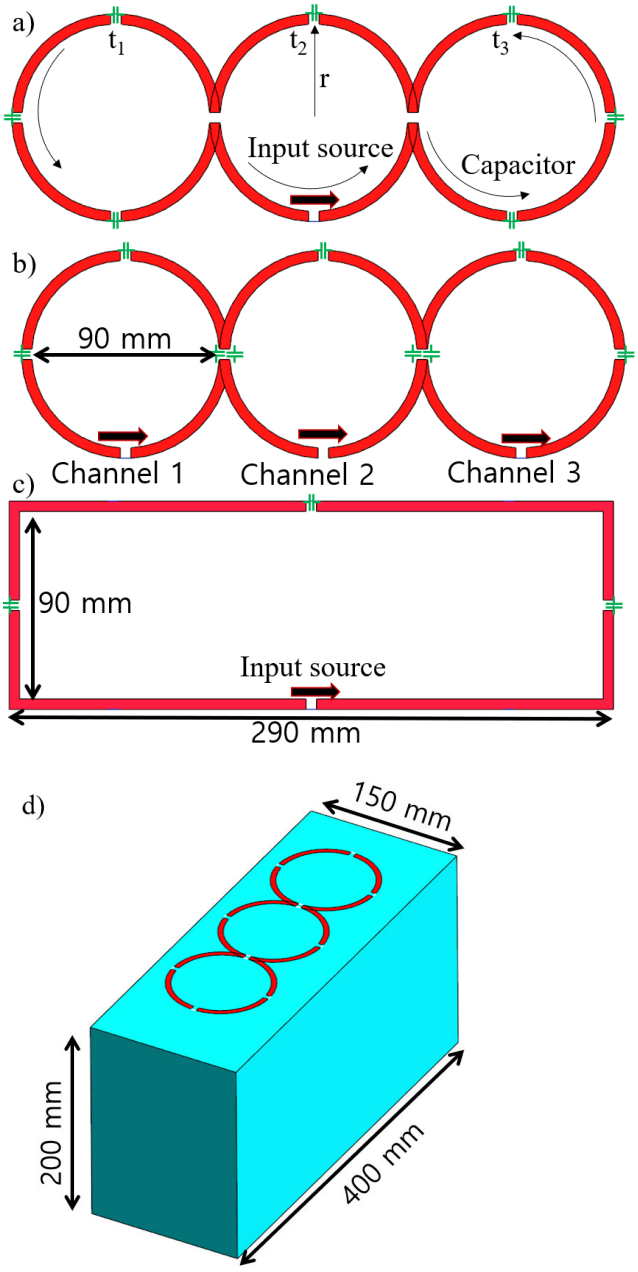

FIGURE 1. Geometry and design of the a) recycle-coil coil using a single channel that indicates the current direction. The comparison and reference coils b) based on three loop array coils, and a c) large rectangular coil. d) the position of recycle-coil with the phantom used in simulations.

each tissue, and the value of each tissue electrical properties was updated according to a central frequency of 300 MHz. These values were provided by the software database, which is based on previous studies [30].

B. SINGLE-CHANNEL SIMULATIONS

The single-channel recycle-coil had an inner radius of r = 45 mm, a conductor line thickness of 5 mm, and n = 3 cycles, as shown in Fig. 1a. The source was placed in the middle cycle. The single-channel recycle-coil used seven capacitors for tuning to 300 MHz. Based on the same geometry, a loop array of three circular elements, referred as array of three channels, was simulated, as shown in Fig. 1b. Each element had an inner radius of 45 mm. The coils were separated in the normal direction by 5 mm. The input source for each channel is shown in Fig. 1b. A large rectangular coil was also simulated, and the geometry is shown in Fig. 1c, which had a length of 290 mm and a width of 90 mm. All the coils were placed along the X-Z plane.

The B1 field and SAR maps were computed inside a rectangular phantom with dimensions of 150 × 200 × 400 mm, as shown in Fig. 1d, which was set with the electrical properties of muscles—conductivity of 0.77 S/m and relative permittivity of 58.20. The coils were placed 10mm from the surface of the phantom.

C. BRAIN ARRAY SIMULATIONS

The performance of the recycle-coil in an array configuration was also investigated. This analysis aimed to demonstrate the possibility of achieving a similar field performance with fewer transmission channels or elements. Based on this analysis, the number of coils can be reduced while maintaining a similar performance.

In this analysis, the reference coil array was based on 24 elements, comprising three rows along the Z-axis and eight elements in each row around the Z-axis, as shown in Fig. 2a. Each circular coil was designed with an inner radius of 40 mm. These coils were then positioned around a cylindrical structure with a diameter of 290 mm to match the dimensions of the head model, extending along a length of 260 mm. The individual coils were arranged to conform to the shape of the cylinder. A separation of 5 mm in the normal plane was used to avoid connections between the coils in each row. The eight coils in the X-Y plane were excited with a phase shift of 45° between adjacent coils to form a uniform B1 field at the center of the coil. The performance of the recycle-coil was demonstrated for two cases: one in which an 8-channel coil array was used, where each channel consists of three cycles, thus covering the same space as the 24-channel reference coil. The recycle-coil consisted of three cycles with an internal radius of 40 mm and was placed around a cylindrical structure of radius and height of 290 and 260 mm, respectively. The geometry and position with reference to the head model are shown in Fig. 2b, where each coil element was assigned an angle of 45° between adjacent coils. The coil configuration of Fig. 2a-b are used for fair comparison since they have the same geometry. Furthermore, we increased the number of elements to 16 to demonstrate the advantages of the proposed coil, as shown in Fig. 2c, in which the coils were arranged around the X-Y plane, following an ellipsoid shape of mayor and minor diameter of 290 and 260 mm, respectively. A phase difference of 22.5° was assigned between adjacent coils. This configuration was different from Fig. 2a-b, in order to demonstrate the capability of the proposed coil to work at different geometric conditions.

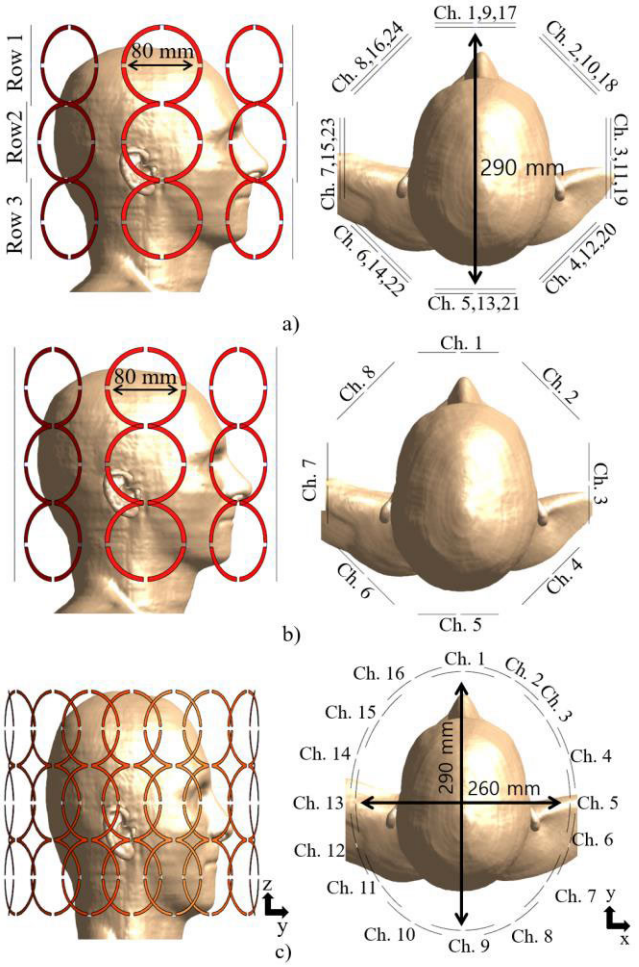

FIGURE 2. Geometry and design of the array of coils for brain imaging, a) the reference array based on 24 loop coils, indicating the number of channels. b) The proposed 8-channels recycle-coil array. c) The 16-channels recycle-coil. The right column images are in the Z-Y plane, whereas the left column row images are in the Y-X plane.

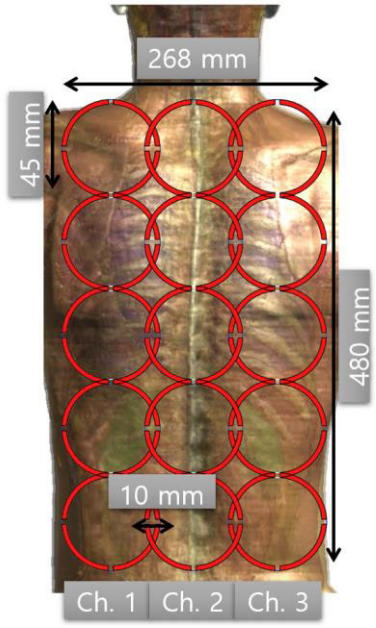

FIGURE 3. Design of the array coil in position with the human torso. The coil array comprises three channels of the proposed recycle-coil coil comprising 5 cycles per channel. The same geometry was used to compare the conventional array coil of 15 elements by adding capacitors to close the loop.

D. SPINE ARRAY SIMULATIONS

We extended the analysis to spinal imaging applications to demonstrate the advantage of the recycle-coil in covering large areas while producing a localized B1 field as a linear array. An array of three elements was designed in which each recycle-coil comprised five cycles with a radius of 45 mm for each cycle. The design of the coil array and its position relative to the spine are shown in Fig. 3. The total coverage area was 268 × 300 mm. The separation between the coil and the human model was 10 mm. An array of 15 circular coils was designed to compare the performance of the recycle-coil. Each coil had a radius of 45 mm and an overlap of 15 mm was applied to reduce the coupling between elements.

E. FIELD NORMALIZATION AND MEASUREMENTS

To ensure a fair comparison between the reference and proposed coils, the acquired B1 field maps were normalized to a value of 2 μT at the center of the coil structure, following the method described in reference [31]. This normalization was achieved by scaling the input power of each coil structure while distributing the power equally among them. The choice of 2 μT was based on the requirement of a rectangular pulse with a duration of 3ms to achieve a flip angle of 90°. By normalizing the input power in this manner, an average specific absorption rate (SAR) of 10g was computed, allowing for a direct comparison between the reference and proposed recycle-coil designs. The fields were compared based on the mean value and the coefficient of variation, which is the standard deviation divided by the mean. A lower value indicates a more uniform field.

F. COIL DEVELOPMENT

The coil was built and tested based on the simulation designs. A picture of the coil is shown in Fig. 4a-b. The coil had a radius of 45 mm and was developed for three and five cycles. The coil was developed using flexible copper tape with a thickness of 5 mm. The coil was tuned with capacitors along its length and a matching circuit based on the capacitor was attached to the source. A reference loop array coil was also used for comparison. This coil consists of 3 transmission channels, and 6 reception channels. The dimensions of the transmission loop coils were 220 by 220mm, and the reception coils were 150 by 110 mm.

G. MR IMAGING

We acquired images using a 7T MRI (Siemens, Magnetom) scanner to test the performance of the proposed coil. Images were captured using a phantom that emulates the spinal cord and torso, as shown in Fig. 4c-d. The phantom was composed

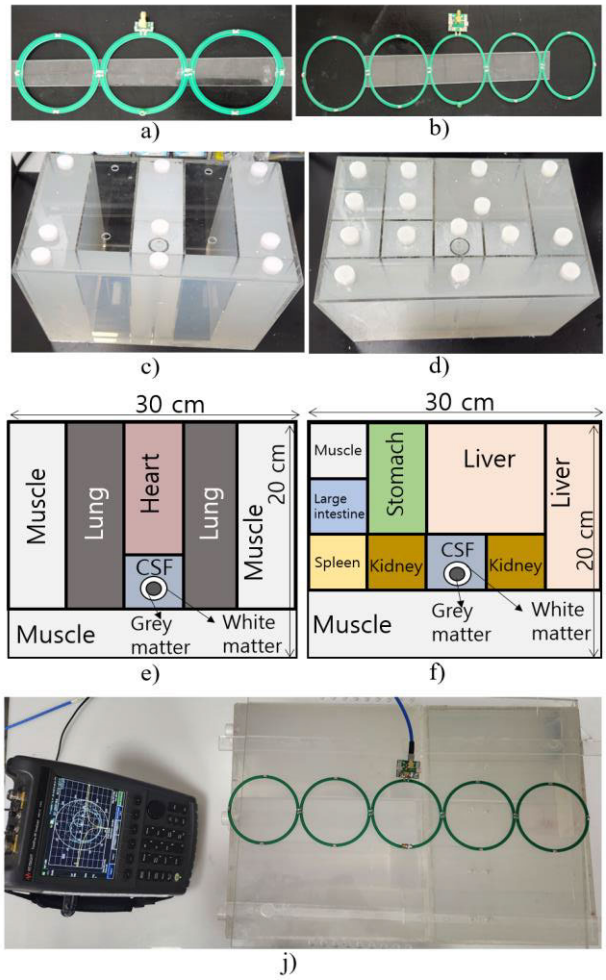

FIGURE 4. Pictures of the developed recycle-coil coil with a) 3 cycles and b) 5 cycles. Pictures of the c,d) developed phantoms for MR images. e,f) Phantoms to simulate the spinal cord and torso, indicating the respective tissues. The j) bench-work measurement setup of the coil with the phantoms.

of a combination of agar, water, sodium, and sucrose for the tissues of the cerebrospinal fluid CSF, muscle, kidney, spleen, stomach, liver, lungs, large intestine, and gray matter, with the corresponding permittivity and conductivity. The phantoms were prepared according to [32] and [33]. The phantom was made from two acrylic cases of 30 × 20 × 20 cm and 30 × 20 × 25 cm for Phantoms 1 and 2, respectively. The tissue distribution is shown in Fig. 4e-f. The two center tubes with diameters of 8 and 4 cm and a length of 20 cm were used to simulate the spinal cord, where the external cylinder had white matter properties, whereas the internal tube had grey matter properties, as shown in the figure. These tubes were surrounded by a section made for CSF. The lung area was maintained empty to simulate the lung area during the torso imaging. Figure 4j shows the picture of the measurement of the S-parameters with the proposed coil and phantom.

III. RESULTS

A. SINGLE-CHANNEL SIMULATION RESULTS

EM simulations were performed to acquire the magnetic B1 field in the phantom based on the aforementioned design. The recycle-coil of Fig. 1a was tuned with capacitors of 4 pF and matched to 50 Ω. Similarly, three single-loop coil arrays and a large rectangular coil were tuned. Notably, because the proposed coil is a single channel, coupling is not considered. However, decoupling should be considered in the case of the array of three channels. Coupling can be reduced by overlapping the coils, which also reduces the coverage area as well. The S21 and S31 parameter values at 300 MHz were −13 and −27 dB, respectively, at the position without overlapping. This situation was considered when the same geometric structure as the recycle-coil was compared.

To demonstrate the current flow of the proposed, recycle-coil, Fig. 5 compares the current density J on the surface of the array of three channels in Fig. 5a and for the recycle-coil in Fig. 5b. It is evident that the recycle coil can produce the same current distribution as that of the three separate channel array coils.

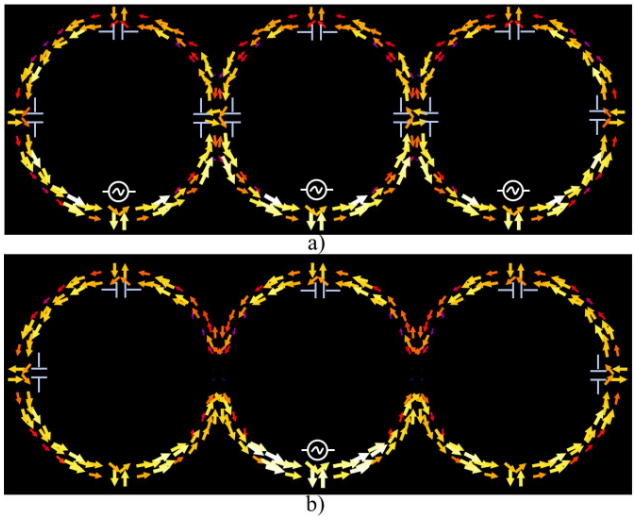

FIGURE 5. The surface current density vector field, for a) 3 loop array coil and b) the recycle coil with 3 cycles.

The B1 fields obtained for each coil structure are presented in Fig. 6, for which the field was normalized to 2 μT at the location marked with a green circle. The B1 field in the X-Y plane at the center of the coil for the large rectangular coil, array of three channels, and recycle-coil is shown in Fig. 6 a-c, respectively. Similarly, the B1 field in the Z-Y plane is shown in Fig. 6 d-f. The line profile was selected as indicated in Fig. 6d and plotted in Fig. 6g, which indicated that the field intensity of the recycle-coil was similar to that of the large rectangular coil, whereas the field intensity of the array of three channels was 30% lower at the selected distances. The mean value and the coefficient of variation of the B1 field at the selected region-of-interest ROI (indicated in the yellow

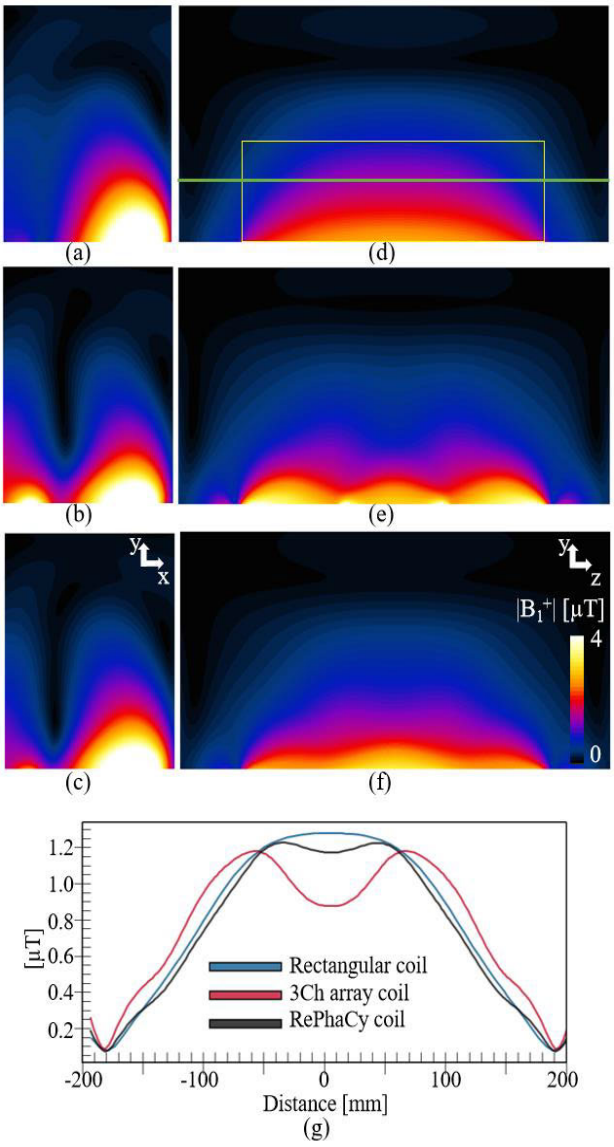

FIGURE 6. Magnetic B1 field maps acquired with the rectangular phantom for the a,d) large rectangular coil, b,e) three loop coil array, and c,f) proposed recycle-coil coil, for the X-Y and Z-Y planes, respectively. The g) line profile along the Z-axis comparing the B1 field distribution produced by each coil.

box in Fig. 6d) for the Z-Y plane was 1.3/0.04, 1.3/0.08, and 1.3/0.01 μT for the large rectangular coil, the array of three channels, and recycle-coil, respectively. Based on these values, the proposed coil can produce a field with a strength similar to that of the reference coils, while maintaining a more uniform field distribution.

A total SAR average of 10g was computed for each coil structure and the maps are shown in Fig. 7a-c for the large rectangular coil, array of three channels, and recycle-coil, respectively. This figure is a maximum intensity projection (MIP) on the Z-Y plane of all maximum values along the X-axis. This is a ray-tracing method that displays the maximum intensity encountered for each ray within volumetric

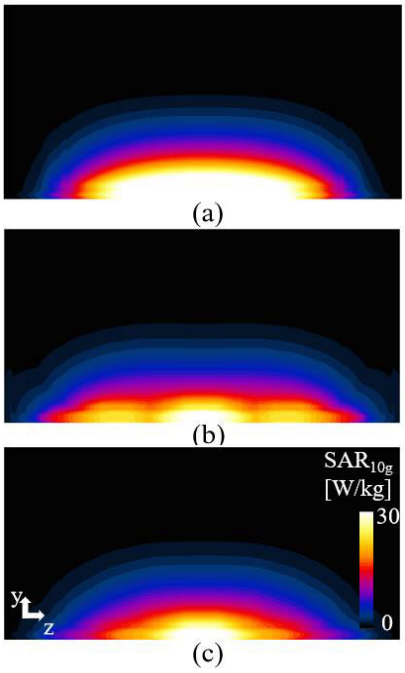

FIGURE 7. Computed SAR with MIP view in the Y-Z plane for a) the large rectangular coil, b) the three loop coil, and c) the proposed recycle-coil.

data projected onto the selected plane. Thus, the location in which the maximum SAR values were present in the entire volume could be visualized. The maximum and mean SAR for the large rectangular coil, array of three channels, and single-channel recycle-coil were 44/1.9, 33/2.3, and 30/1.2, respectively. Thus, the use of the recycle-coil can improve the B1 field uniformity by 25% compared with the array of three channels, whereas the maximum SAR was reduced by 31% compared with the large rectangular coil.

B. BRAIN ARRAY SIMULATION RESULTS

The coupling analysis based on the S1j-parameter of the 24-channel loop coil array and 8-channel recycle-coil is plotted in Fig. 8a-b, respectively. In the case of the 24-channel loop coil array, the Sij parameter exhibited a range of -41 dB to -8 dB, indicating the presence of coupling between the coils. This highlights the importance of implementing decoupling methods to mitigate the coupling effects. On the other hand, when the recycle-coil was used, the coupling was significantly reduced, with Sij parameter values ranging from -60 dB to -20 dB. The recycle-coil design demonstrates improved decoupling performance, reducing the need for additional decoupling methods.

The magnetic fields acquired using the 24-channels loop coil array, 8-channels recycle-coil, and 16-channels recycle-coil are shown in Fig. 9a-c. The left, middle, and right columns show the field in the X-Y plane of the center of the coil, the area of the lateral ventricles in the brain area, and the Z-Y plane at the center of the coil, respectively. All B1 fields were normalized to obtain 2 μT at the isocenter of

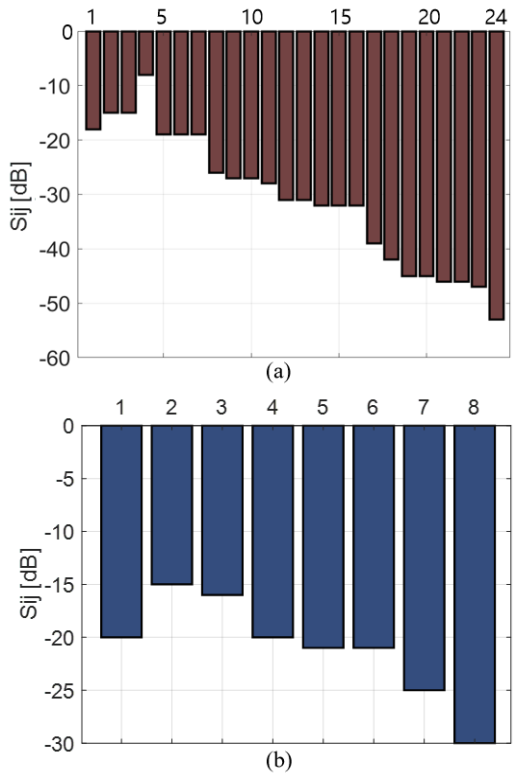

FIGURE 8. The coupling analysis based on Sij for the a) 24-channels loop coils array and b) 8-channel recycle coil.

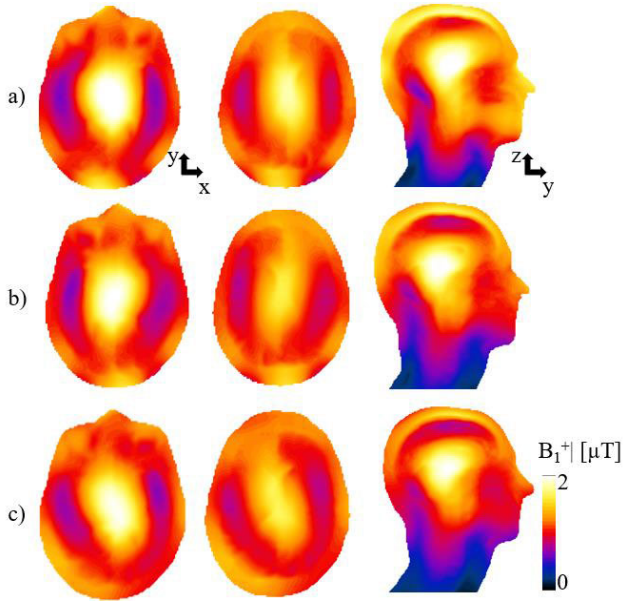

FIGURE 9. Computed B_1 fields of the brain for a) the 24-channel loop array coil, b) the 8-channels recycle-coil array, and c) the 16-channels recycle-coil array. The first and second columns are for the X-Y plane, whereas the third column is for the Z-Y plane.

the coil. The input power was scaled to achieve the target magnitude. The mean and the coefficient of variation for the X-Y slice at the ventricle (middle column of Fig. 9) was 1.17/0.05, 1.14/0.03, and 1.15/0.04 μT, for the reference 24-channels loop coil array, 8-channels recycle-coil, and the 16-channels recycle-coil array, respectively. From the field maps, the 24-channels loop coil array and 8-channels recycle-coil exhibit similar performances, and the use of the recycle-coil coil reduces the use of multiple transmit and reception channels.

The average SAR 10 g maps for the 24-channels loop coil array, 8-channels recycle-coil, and 16-channels recycle-coil arrays are shown in Fig. 10a-c, respectively. The SAR maps shown in the first and second columns are the X-Y planes at the center of the coil and ventricle area, respectively. The third column shows the MIP SAR in the Z-Y view projected along the X-axis. The green line indicates the position of the slice with the maximum SAR, which is shown in the X-Y plane in the fourth plane where the maximum SAR value was present. The maximum and mean SAR in the entire head volume for each structure was 4.1/0.66, 3.51/0.55, and 3.2/0.10 W/kg, for the 24-channels loop coil array, 8-channels recycle-coil, and the 16-channels recycle-coil array, respectively. Thus, the proposed coil can produce a field intensity similar to that of multiple single-coil element arrays but with the advantage of lower SAR.

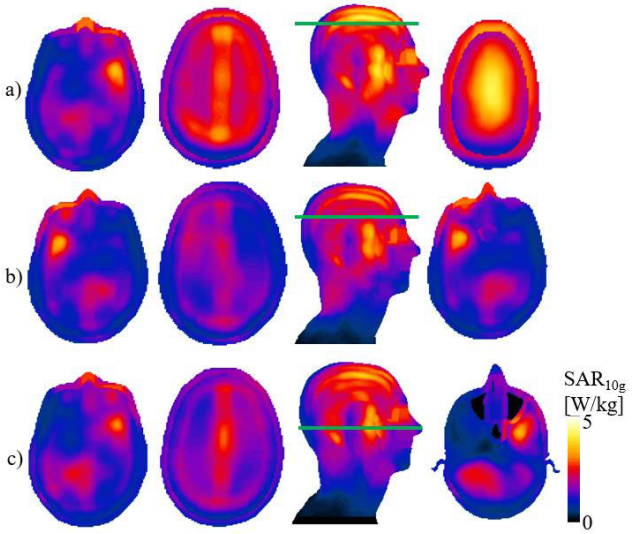

FIGURE 10. Computed SAR for a) the 24-channel loop array coil, b) the 8-channels recycle-coil array, and c) the 16-channels recycle-coil array. The first and second column shows the X-Y plane at the center of the coil and at the ventricle of the brain. The third column is the Z-Y MIP view, indicating the slice with the maximum SAR, which is shown in the fourth column.

C. SPINE ARRAY SIMULATION RESULTS

The magnetic field was computed in the torso with the reference of 15-channels loop array, which is shown in Fig. 11a-c and the 3-channels recycle-coil array is shown in Fig. 11d-f. The field maps were normalized to 2 μT at the center of the coil along the Z-axis and on the Y-axis at the position of the spinal cord, as shown using the circle in Fig. 11a. The field in the X-Y plane is shown in Fig. 11a,d at

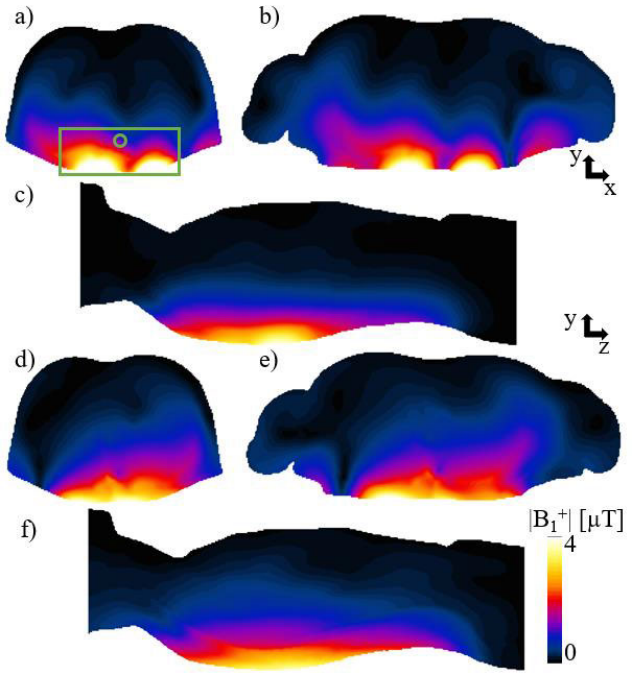

FIGURE 11. Computed B_1 field a-c) using the 15-channel array coil and d-f) using the 3-channels recycle-coil array, for the X-Y plane at the center of the coil, at V5 of the spine, and the Z-Y plane, respectively.

the center of the coil, whereas Fig. 11b,e shows the fields at the T5 vertebra of the spinal cord. The B1 fields in the Z-Y plane are shown in Fig. 11c,d for the 15-channels loop array and 3-channels recycle-coil array, respectively. The green rectangle in Fig. 11a indicates the ROI used to compute the statistics of the fields in the human model. The mean and the coefficient of variation on this slice were 1.9/0.3 and 1.8/0.11 μT for the 15 and 3ch array, respectively.

Both the 15-channel loop array and 3-channel recycle-coil array exhibited an average specific absorption rate (SAR) of 10 g, as depicted in Fig. 12. The maximum intensity projection (MIP) views of the SAR in the Y-Z plane are illustrated in Fig. 12a and 12c for the 15-channel loop array and 3-channel recycle-coil array, respectively. Fig. 12b and 12d showcase the X-Y plane with the maximum SAR values for the 15-channel loop array and 3-channel recycle-coil array, respectively. The maximum SAR values were measured at 32/1.36 W/kg for the 15-channel loop array and 18/0.85 W/kg for the 3-channel recycle-coil array. The mean SAR values were 1.36 W/kg and 0.85 W/kg for the 15-channel loop array and 3-channel recycle-coil array, respectively.

Notably, the maximum SAR of the proposed coil was reduced by 43% compared with the reference coil, whereas a similar B1 field intensity and a higher uniformity were achieved using the proposed coil.

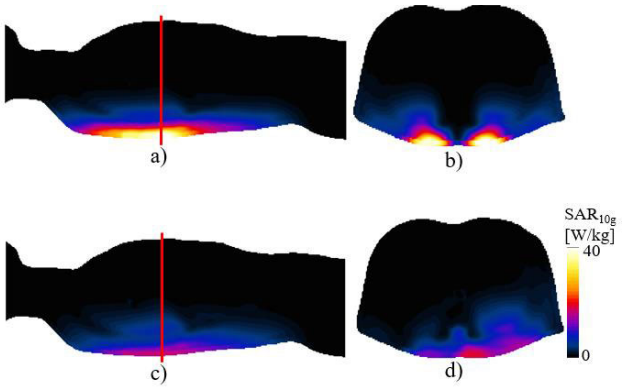

FIGURE 12. Computed average SAR of 10 g, for the a,b) 15-channel loop array coil and c,d) for the 3-channels recycle-coil array. The Z-Y plane with the MIP view indicates the position of the slice with maximum SAR in red. And in the last column the X-Y plane view of the corresponding coils.

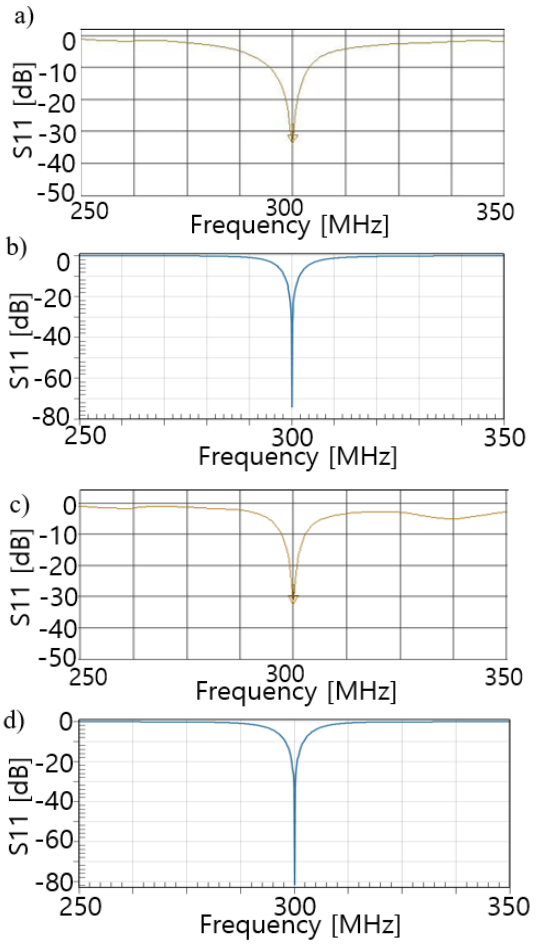

FIGURE 13. The S11 parameters from the built and simulated recycle-coil with 3 turns a) measured, b) simulated, and for the 5 turn recycle-coil for c) measured and d) simulated.

D. COIL BENCHWORK

The proposed coil was built according to the geometry and design shown in Fig. 4a-b. The coils with three and five cycles were tuned with capacitors of 2.2 and 4.1 pF, respectively, with the addition of a variable capacitor at the center cycle for fine-tuning. The capacitors were chosen through an empirical process to obtain a low peak value of S11 at the target frequency of 297.4 MHz. The measured

and simulated S11 parameters after tuning and matching the recycle-coil with three turns are shown in Fig. 13 a-b and the recycle-coil with five turns are shown in Fig 13 c-d, respectively. The bandwidth of the built coil matching circuit was 1 MHz.

E. MRI IMAGES

MR images were obtained using the target phantoms with a turbo spin echo pulse sequence with repetition and echo times of 1200.0 and 7.3 ms, respectively, a flip angle of 90°, and a slice thickness of 2 mm for a 256 × 256 matrix. Images in the sagittal and axial orientations were acquired. The images shown in Fig. 14a-b were acquired using the reference coil, whereas images acquired with the recycle-coil with 3 cycles and 5 cycles are shown in Fig. 14 c-d and Fig. 14 e-f, for axial and sagittal view, respectively. The red square indicates the region where the standard deviation was measured, and the yellow boxes show the place where the mean value was computed to calculate the SNR of each image.

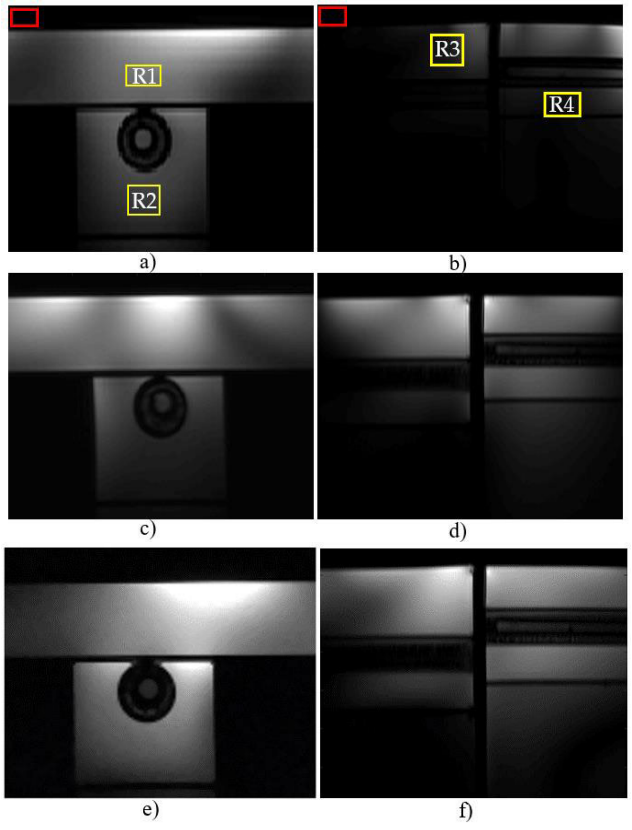

FIGURE 14. Acquired MR images, with the reference coil a) axial and b) sagittal view. The MR images with the 3 cycles in c) axial and, d) sagittal view, and the coil with 5 cycles in e) axial and f) sagittal view.

The SNR for the axial view for the R1/R2 is 25/11, 28/4 and 32/17, for the reference coil, 3- and 5-cycle recycle-coil arrays, respectively. In the same manner the SNR for the ROI R3/R4 in the sagittal view were 55/17, 95/57, 107/76, for the reference coil, 3- and 5-cycle recycle-coil arrays, respectively. It can be seen that the proposed 5-cycle recycle coil can provide higher SNR and image quality than the reference coil. The 5-cycle recycle coil has an SNR of almost two times larger than the reference coil while the 3-cycle recycle coil had 70% better SNR than the reference coil.

IV. DISCUSSIONS

This study proposed the design of an extension of a loop coil that could improve the spatial resolution of small loop coils while providing a focused and localized B1 field similar to a small loop coil. The concept of the proposed coil was based on the recycling and rephasing of current, which was achieved by modifying the current path along the coil. We performed simulations, and MR images were obtained after the coil was built. Through simulations, we observed that the proposed coil could provide a localized and strong field similar to an array of small-loop coils while maintaining a reduced SAR compared with an array of small coils. particularly, the proposed coil could provide a large spatial range, as demonstrated by spine simulations. The proposed coil concept could free the use of channels; therefore, it could be added to other positions to improve the field intensity or image quality. Practically, the use of this coil reduced the complexity of decoupling each coil. Based on the simulations, the magnetic fields of the reference and proposed coils were similar; however, the maximum SAR was reduced by 43% when the proposed coil design was applied to the spine. The number of channels required to acquire the field was reduced from 15 to 3. A limitation of the proposed coil is its capability to perform parallel imaging in the direction of the coil position. Another limitation of the present work is that we did not conduct in vivo experiments in this study owing to the failure to obtain institutional review board IRB approval. The proposed coil can be extended to the extremes and torso imaging as well as various MRI field strengths, such as 1.5 and 3T. In future studies we plan to perform in vivo experiments and apply it to different applications such as animal imaging or preclinical studies.

REFERENCES

[1] E. J. R. van Beek, C. Kuhl, Y. Anzai, P. Desmond, R. L. Ehman, Q. Gong, G. Gold, V. Gulani, M. Hall-Craggs, T. Leiner, C. C. T. Lim, J. G. Pipe, S. Reeder, C. Reinhold, M. Smits, D. K. Sodickson, C. Tempany, H. A. Vargas, and M. Wang, "Value of MRI in medicine: More than just another test?" *J. Magn. Reson. Imag.*, vol. 49, no. 7, pp. e14–e25, 2019.

[2] A. Saifuddin and R. A. R. Green, "Whole spine MRI in the assessment of acute vertebral body trauma," *Skeletal Radiol.*, vol. 33, no. 3, pp. 129–135, Mar. 2004.

[3] Z. Li, Y. A. Chen, D. Chow, J. Talbott, C. Glastonbury, and V. Shah, "Practical applications of CISS MRI in spine imaging," *Eur. J. Radiol. Open*, vol. 6, pp. 231–242, 2019.

[4] A. Bozzo, J. Marcoux, M. Radhakrishna, J. Pelletier, and B. Goulet, "The role of magnetic resonance imaging in the management of acute spinal cord injury," *J. Neurotrauma*, vol. 28, no. 8, pp. 1401–1411, Aug. 2011.

[5] L. S. Honig and W. A. Sheremata, "Magnetic resonance imaging of spinal cord lesions in multiple sclerosis," *J. Neurol., Neurosurg. Psychiatry*, vol. 52, no. 4, pp. 459–466, 1989.

[6] M. Wassenaar, R. M. van Rijn, M. W. van Tulder, A. P. Verhagen, D. A. W. M. van der Windt, B. W. Koes, M. R. de Boer, A. Z. Ginai, and R. W. J. G. Ostelo, "Magnetic resonance imaging for diagnosing lumbar spinal pathology in adult patients with low back pain or sciatica: A diagnostic systematic review," *Eur. Spine J.*, vol. 21, no. 2, pp. 220–227, Feb. 2012.

[7] O. Kraff and H. H. Quick, "7T: Physics, safety, and potential clinical applications," *J. Magn. Reson. Imag.*, vol. 46, no. 6, pp. 1573–1589, Dec. 2017.
[8] A. G. Van der Kolk, J. Hendrikse, J. J. M. Zwanenburg, F. Visser, and P. R. Luijten, "Clinical applications of 7 T MRI in the brain," *Eur. J. Radiol.*, vol. 82, no. 5, pp. 708–718, 2013.
[9] O. Kraff, A. Fischer, A. M. Nagel, C. Mönninghoff, and M. E. Ladd, "MRI at 7 Tesla and above: Demonstrated and potential capabilities," *J. Magn. Reson. Imag.*, vol. 41, no. 1, pp. 13–33, Jan. 2015.
[10] S.-M. Sohn, L. DelaBarre, J. T. Vaughan, and A. Gopinath, "RF multichannel head coil design with improved $B1^+$ fields uniformity for high field MRI systems," in *IEEE MTT-S Int. Microw. Symp. Dig.*, Jun. 2012, pp. 1–3.
[11] C. M. Deniz, R. Brown, R. Lattanzi, L. Alon, D. K. Sodickson, and Y. Zhu, "Maximum efficiency radiofrequency shimming: Theory and initial application for hip imaging at 7 Tesla," *Magn. Reson. Med.*, vol. 69, no. 5, pp. 1379–1388, May 2013.
[12] K. Ugurbil, "Magnetic resonance imaging at ultrahigh fields," *IEEE Trans. Biomed. Eng.*, vol. 61, no. 5, pp. 1364–1379, May 2014.
[13] B. van den Bergen, C. A. T. Van den Berg, L. W. Bartels, and J. J. W. Lagendijk, "7 T body MRI: B1 shimming with simultaneous SAR reduction," *Phys. Med. Biol.*, vol. 52, no. 17, pp. 5429–5441, Sep. 2007.
[14] B. van den Bergen, C. A. T. van den Berg, D. W. J. Klomp, and J. J. W. Lagendijk, "SAR and power implications of different RF shimming strategies in the pelvis for 7T MRI," *J. Magn. Reson. Imag.*, vol. 30, no. 1, pp. 194–202, Jul. 2009.
[15] H. Homann, I. Graesslin, H. Eggers, K. Nehrke, P. Vernickel, U. Katscher, O. Dössel, and P. Börnert, "Local SAR management by RF shimming: A simulation study with multiple human body models," *Magn. Reson. Mater. Phys., Biol. Med.*, vol. 25, no. 3, pp. 193–204, Jun. 2012.
[16] D. Hernandez, Y. Han, S. Son, and K.-N. Kim, "Design of microstrip transmission line array for magnetic resonance imaging at 300 MHz for spinal cord examination," *J. Electromagn. Waves Appl.*, vol. 35, no. 9, pp. 1125–1139, Jun. 2021.
[17] D. Hernandez, T. Nam, Y. Jeong, D. Kim, and K.-N. Kim, "Study on the effect of non-symmetrical current distribution controlled by capacitor placement in radio-frequency coils for 7T MRI," *Biosensors*, vol. 12, no. 10, p. 867, Oct. 2022.
[18] W. Zhao, J. Cohen-Adad, J. R. Polimeni, B. Keil, B. Guerin, K. Setsompop, P. Serano, A. Mareyam, P. Hoecht, and L. L. Wald, "Nineteen-channel receive array and four-channel transmit array coil for cervical spinal cord imaging at 7 Tesla," *Magn. Reson. Med.*, vol. 72, no. 1, pp. 291–300, Jul. 2014.
[19] M. W. May, S. J. D. Hansen, M. Mahmutovic, A. Scholz, N. Kutscha, B. Guerin, J. P. Stockmann, R. L. Barry, E. Kazemivalipour, R. Gumbrecht, R. Kimmlingen, M. Adriany, Y. Chang, C. Triantafyllou, S. Knake, L. L. Wald, and B. Keil, "A patient-friendly 16-channel transmit/64-channel receive coil array for combined head–neck MRI at 7 Tesla," *Magn. Reson. Med.*, vol. 88, no. 3, pp. 1419–1433, Sep. 2022.
[20] B. Gruber, M. Froeling, T. Leiner, and D. W. J. Klomp, "RF coils: A practical guide for nonphysicists," *J. Magn. Reson. Imag.*, vol. 48, no. 3, pp. 590–604, Sep. 2018.
[21] D. Hernandez and K.-N. Kim, "A review on the RF coil designs and trends for ultra high field magnetic resonance imaging," *Investigative Magn. Reson. Imag.*, vol. 24, no. 3, p. 95, 2020.
[22] K.-N. Kim, D. Hernandez, J.-H. Seo, Y. Noh, Y. Han, Y. C. Ryu, and J.-Y. Chung, "Quantitative assessment of phased array coils with different numbers of receiving channels in terms of signal-to-noise ratio and spatial noise variation in magnetic resonance imaging," *PLoS ONE*, vol. 14, no. 7, Jul. 2019, Art. no. e0219407.
[23] C. E. Hayes and L. Axel, "Noise performance of surface coils for magnetic resonance imaging at 1.5 T," *Med. Phys.*, vol. 12, no. 5, pp. 604–607, Sep. 1985.
[24] A. Kumar, A. E. William, and A. B. Paul, "Noise figure limits for circular loop MR coils," *Magn. Reson. Med.*, vol. 61, no. 5, pp. 1201–1209, 2009.
[25] A. Kuehne, S. Goluch, P. Waxmann, F. Seifert, B. Ittermann, E. Moser, and E. Laistler, "Power balance and loss mechanism analysis in RF transmit coil arrays," *Magn. Reson. Med.*, vol. 74, no. 4, pp. 1165–1176, Oct. 2015.
[26] J. Hamilton, D. Franson, and N. Seiberlich, "Recent advances in parallel imaging for MRI," *Prog. Nucl. Magn. Reson. Spectrosc.*, vol. 101, pp. 71–95, Aug. 2017.
[27] U. Katscher and P. Börnert, "Parallel RF transmission in MRI," *NMR Biomed.*, vol. 19, no. 3, pp. 393–400, May 2006.
[28] J. Felder, C.-H. Choi, Y. Ko, and N. J. Shah, "Optimization of high-channel count, switch matrices for multinuclear, high-field MRI," *PLoS ONE*, vol. 15, no. 8, Aug. 2020, Art. no. e0237494.
[29] M.-C. Gosselin, E. Neufeld, H. Moser, E. Huber, S. Farcito, L. Gerber, M. Jedensjö, I. Hilber, F. D. Gennaro, B. Lloyd, E. Cherubini, D. Szczerba, W. Kainz, and N. Kuster, "Development of a new generation of high-resolution anatomical models for medical device evaluation: The virtual population 3.0," *Phys. Med. Biol.*, vol. 59, no. 18, pp. 5287–5303, Sep. 2014.
[30] S. Gabriel, R. W. Lau, and C. Gabriel, "The dielectric properties of biological tissues: II. Measurements in the frequency range 10 Hz to 20 GHz," *Phys. Med. Biol.*, vol. 41, no. 11, pp. 2251–2269, Nov. 1996.
[31] C. M. Collins and M. B. Smith, "Signal-to-noise ratio and absorbed power as functions of main magnetic field strength, and definition of '90°' RF pulse for the head in the birdcage coil," *Magn. Reson. Med.*, vol. 45, no. 4, pp. 684–691, Apr. 2001.
[32] Q. Duan, J. H. Duyn, N. Gudino, J. A. de Zwart, P. van Gelderen, D. K. Sodickson, and R. Brown, "Characterization of a dielectric phantom for high-field magnetic resonance imaging applications," *Med. Phys.*, vol. 41, no. 10, Oct. 2014, Art. no. 102303.
[33] D. Hernandez and K.-N. Kim, "Correlation analysis between the complex electrical permittivity and relaxation time of tissue mimicking phantoms in 7 T MRI," *Sci. Rep.*, vol. 12, no. 1, pp. 1–12, Sep. 2022.

DANIEL HERNANDEZ received the Ph.D. degree from Kyung Hee University, Republic of Korea, in 2016. He is currently a Researcher and an Assistant Professor with the Department of Biomedical Engineering, Gachon University. His current research interests include electromagnetic theory, simulations and development of antennas, and image and signal processing for MRI engineering.

DONGHYUK KIM received the Ph.D. degree from the Department of Health Sciences and Technology, Gachon University, Incheon, Republic of Korea, in 2022. He is currently a Research Professor with the Neuroscience Research Institute, Gachon University. His current research interests include RF coil design and analysis of electromagnetic fields.

TAEWOO NAM received the M.S. degree from the Department of Health Sciences and Technology, Gachon University, Incheon, Republic of Korea, in 2022, where he is currently pursuing the Ph.D. degree. His current research interests include ultra-high field RF MRI coils, electromagnetic field simulation, and RF circuitry design.

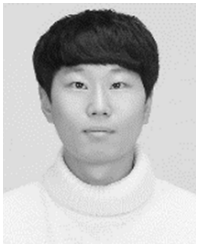

YONGHWA JEONG received the M.S. degree from the Department of Health Sciences and Technology, Gachon University, Incheon, Republic of Korea, in 2023. He is currently a Researcher with the Neuroscience Research Institute, Incheon. His current research interests include RF array antenna and electrical property tomography at high-field MRI.

MINYEONG SEO received the M.S. degree from the Department of Health Sciences and Technology, Gachon University, Incheon, Republic of Korea, in 2022. She is currently a Researcher with the Neuroscience Research Institute, Incheon. Her current research interests include RF array coil, magnetic field monitoring probe, and electromagnetic analysis.

EUNWOO LEE is currently pursuing the B.Sc. degree with the Department of Biomedical Engineering, Gachon University. Her current research interests include deep learning applications in magnetic resonance imaging, RF/microwave exposure, and electromagnetic field simulation.

JUNGHWAN KIM received the Ph.D. degree in bioengineering from the University of Pittsburgh, PA, USA, in 2018. He has been an Assistant Professor with the Department of Radiology and Electrical Engineering and Computer Science, University of Missouri-Columbia, Columbia, MO, USA, since 2021. His current research interests include MRI hardware, EM analysis, antenna development, and imaging analysis.

KYOUNG-NAM KIM received the Ph.D. degree in electrical engineering and information technology from the University of Duisburg–Essen, Germany, in 2011. He has been an Associate Professor with the Department of Biomedical Engineering, Gachon University, Inchon, Republic of Korea, since 2016. His current research interests include medical electronic engineering, MRI systems, electromagnetic field analysis, RF/microwave safety, and RF MRI coils. He is currently an MRI Committee Member of the Korean Society of Magnetic Resonance in Medicine.